Comparison of Arterial Spin Labeling and First-Pass Dynamic Contrast-Enhanced MR Imaging in the Assessment of Pulmonary Perfusion in Humans: The Inflow Spin-Tracer Saturation Effect

Yi-Ru Lin,[1,2] Ming-Ting Wu,[2,3,*] Teng-Yi Huang,[4] Shang-Yueh Tsai,[1] Hsiao-Wen Chung,[1,5] Vu M. Mai,[6] Cheng-Yu Chen,[5] and Huay-Ben Pan[2,3]

The flow-sensitive alternating inversion recovery (FAIR) and the first-pass dynamic contrast-enhanced MR imaging (CE-MRI) techniques have both been shown to be effective in the assessment of human pulmonary perfusion. However, no comprehensive comparison of the measurements by these two methods has been reported. In this study, healthy adults were recruited, with FAIR and CE-MRI performed for an estimation of the relative pulmonary blood flow (rPBF). Regions of interest were encircled from the right and left lungs, with right-to-left rPBF ratios calculated. Results indicated that, on posterior coronal slices, the rPBF ratios obtained with the FAIR technique agreed well with CE-MRI measurements (mean difference = −0.02, intraclass correlation coefficient $R_I = 0.78$, 95% confidence interval = [0.67, 0.86]). On middle coronal slices, however, FAIR showed a substantially lower rPBF by up to 43% in the right lung compared with CE-MRI (mean difference = −0.38, $R_I = 0.34$, 95% confidence interval = [−0.09, 0.68]). The location-dependent discrepancy between measurements by FAIR and CE-MRI methods is attributed to tracer saturation effects of arterial inflow when the middle coronal slice contains the in-plane-oriented right pulmonary artery, whereas the left lung rPBF is less affected due to oblique orientation of the left pulmonary artery. Intrasequence comparison on additional subjects using FAIR at different slice orientations supported the above hypothesis. It is concluded that FAIR imaging for pulmonary perfusion in the coronal plane provides equivalent rPBF information with CE-MRI only in the absence of tracer saturation effects; hence, FAIR should be carefully exercised to avoid misleading interpretations. Magn Reson Med 52:1291–1301, 2004. © 2004 Wiley-Liss, Inc.

Assessment of pulmonary perfusion in clinical practice has traditionally been performed by nuclear medicine scintigraphy using radioactive isotopes such as the Tc99m-labeled macroaggregated albumin (Tc99m-MAA) (1). In recent years, MR imaging emerged as an attractive alternative for such a purpose (2–5). MR imaging has the advantages of simultaneous acquisition of high-resolution anatomic images, multiple functional information to assist diagnosis, and no ionization radiation exposure. Research studies have further shown that MR is able to detect perfusion deficits due to pulmonary embolism (3,6) and that MR provides consistent information compared with perfusion scintigraphy, which is regarded as the current clinical standard (7,8). It is thus clear that MR imaging may have the potential to become one of the routine clinical modalities for screening or monitoring pulmonary diseases.

Among the pulmonary perfusion MR imaging techniques reported to date employing the proton nuclei, the flow-sensitive alternating inversion recovery (FAIR) approach based on arterial spin labeling (9–11) and the first-pass dynamic contrast-enhanced MR imaging (CE-MRI) using i.v. injection of Gd-based contrast agents (2,3,6,7,12,13) seem to hold strong promise in direct clinical applications. The FAIR approach, like other similar arterial spin labeling methods, does not necessitate injection of contrast agents (4,10,14); hence, it is completely noninvasive and allows multiple measurements (15). Recent development incorporating inhalation of oxygen further allows ventilation-perfusion scans to be performed in a single examination without contrast administration (11). On the other hand, dynamic CE-MRI utilizing rapid bolus injection of contrast agents is advantageous in situations where tissue transit time and pulmonary blood volume are to be obtained to assist diagnosis (3,7,16). Measurement of lung perfusion by CE-MRI has been validated by experimental studies using animal models with invasive microsphere measurements as the standard (13,17). Furthermore, first-pass dynamic CE-MRI usually takes less than a minute of scan time and is hence appropriate for clinical studies.

[1]Department of Electrical Engineering, National Taiwan University, Taipei, Taiwan, Republic of China.

[2]Department of Radiology, Kaohsiung Veterans General Hospital, KaoHsiung, Taiwan, Republic of China.

[3]Faculty of Medicine, School of Medicine, National Yang Ming University, Taipei, Taiwan, Republic of China.

[4]Department of Electrical Engineering, National Taiwan University of Science and Technology, Taipei, Taiwan, Republic of China.

[5]Department of Radiology, Tri-Service General Hospital, Taipei, Taiwan, Republic of China.

[6]Evanston Hospital, Evanston Northwestern Healthcare, Evanston, Illinois.

*Correspondence to: Ming-Ting Wu, Section of Thoracic Imaging and MRI, Department of Radiology, Kaohsiung Veterans General Hospital, No.386, Ta-Chung 1st Road, KaoHsiung, Taiwan 813, Republic of China. E-mail: mtwu@isca.vghks.gov.tw

Although CE-MRI and FAIR are both able to assess regional lung perfusion, their mechanisms are quite different. However, there have been only few reports comparing the measurement of regional pulmonary perfusion by these two methods (14). We hypothesize that FAIR of lung, unlike its applications in the brain, may be more complicated due to major arterial inflow contained in the region of interest. Therefore, we attempt to compare the measurements of regional pulmonary perfusion assessed by FAIR and the CE-MRI techniques in healthy human adults. The specific aim of this study is to investigate the suitability of the FAIR perfusion estimation method at different coronal slice locations. Note that coronal slice orientation is investigated here because the coronal view provides better comparison between the right and left lungs, as commonly seen in chest radiographs or lung perfusion scintigrams. In addition, a weakness inherent in the FAIR technique that tends to result in underestimation of pulmonary blood flow in the right lung is reported and its reasons are experimentally investigated.

MATERIALS AND METHODS

Theory

Consider the time evolution of the longitudinal magnetization within an image voxel, $M(t)$, given by the modified Bloch equation including the effects from arterial blood inflow and venous blood outflow:

$$\frac{dM(t)}{dt} = \frac{M_0 - M(t)}{T_1} + fM_A(t) - fM_V(t), \qquad [1]$$

where M_0 is the longitudinal magnetization at thermal equilibrium per gram of tissue, T_1 is the longitudinal relaxation time, f is the capillary blood flow in units of milliliter of blood per second per gram of tissue, and $M_A(t)$ and $M_V(t)$ are the longitudinal magnetization per milliliter of blood in the arteries and veins, respectively. In an arterial spin labeling experiment where the upstream inflow spins are fully saturated, $M_A(t) = 0$. If one further assumes a single compartment model, where the proportions of the labeled spins are identical for the image voxel and for the venous outflow, $M_V(t) = M(t)/\lambda$ with λ being the tissue/blood water partition coefficient. Equation [1] thus becomes

$$\frac{dM(t)}{dt} = \frac{M_0 - M(t)}{T_1} - \frac{f}{\lambda} M(t). \qquad [2]$$

Solving for the modified Bloch equation yields

$$M(t) = \frac{T_{1app}}{T_1} M_0 + \left(1 - \frac{T_{1app}}{T_1}\right) M_0 e^{-t/T_{1app}}, \qquad [3]$$

where

$$T_{1app} = \left(\frac{1}{T_1} + \frac{f}{\lambda}\right)^{-1} \qquad [4]$$

is the apparently shortened longitudinal relaxation time in the presence of inflow with saturated spins. Substitution of $t = 0$ and $t \to \infty$ into Eq. [3] yields, after some manipulation,

$$f = \frac{\lambda}{T_{1app}} \frac{M_0 - M^{ss}}{M_0}, \qquad [5]$$

where M^{ss} stands for the longitudinal magnetization at the steady state (i.e., $t \to \infty$ in Eq. [3]). Equation [5] forms the basis of all arterial spin labeling methods, in which the blood flow f can be estimated on a voxel-by-voxel basis by subtracting the image obtained with labeled arterial flow (M^{ss}) from the image obtained without labeling (M_0).

Being one of the variants of the arterial spin labeling methods, the principle of FAIR imaging for an assessment of tissue perfusion is based on the difference in signal intensity between two images acquired using selective versus nonselective inversion-recovery preparation and otherwise identical scanning parameters (9). In a slice-selective inversion-recovery scan, the blood flow into the image slice and subsequent capillary/tissue water exchange cause a signal change proportional to the perfusion (i.e., the tagged image). In contrast, the inflowing blood results in no signal changes in image acquisition with nonselective inversion (i.e., the control image). Consequently, a subtraction of the tagged and control images yields a perfusion map reflecting regional blood flow, in a manner analogous to Eq. [5]. Note that an important prerequisite for successful applications of the FAIR method is that the inflowing blood should be clearly separable from the image slice in the tagged and control images. If the image slice contained part of the upstream vessels, the inflowing blood would become a mixture of inverted and noninverted spins in the tagged scan. In other words, some of the endogenous tracer becomes indistinguishable to the static tissue in the image slice, causing possible reduction in perfusion-related signal changes.

Assuming that the upstream artery exhibits a proportion β lying within the image slice ($0 < \beta < 1$), these arterial spins would not experience any saturation before being excited by the imaging RF pulse. Equation [2] hence becomes

$$\frac{dM'(t)}{dt} = \frac{M_0 - M'(t)}{T_1} + \frac{f\beta}{\lambda} M_0 - \frac{f}{\lambda} M(t), \qquad [6]$$

where we have denoted the longitudinal magnetization as $M'(t)$ to distinguish from the original $M(t)$ in Eq. [1]. Solving for the modified Bloch equation yields

$$M'(t) = \frac{T_{1app}}{T_\beta} M_0 + \left(1 - \frac{T_{1app}}{T_\beta}\right) M_0 e^{-t/T_{1app}} \qquad [7]$$

where

$$T_\beta = \left(\frac{1}{T_1} + \frac{f\beta}{\lambda}\right)^{-1}. \qquad [8]$$

Clearly, the time evolution of the longitudinal magnetization as expressed in Eq. [7] is no longer identical to that in Eq. [3]. If one still used Eq. [5] to estimate the tissue blood flow f, one would obtain

$$f' = \frac{\lambda}{T_{1app}} \frac{M_0 - M'^{ss}}{M_0} = \lambda \left(\frac{1}{T_{1app}} - \frac{1}{T_\beta}\right) = (1 - \beta)f. \qquad [9]$$
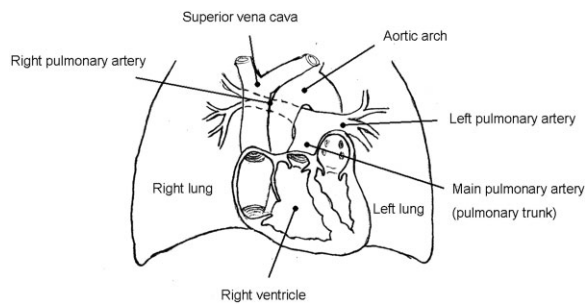
FIG. 1. Schematic drawing of the relative locations of the main pulmonary artery from the right ventricle and the right and left pulmonary arteries. These three vessels are oriented along very different directions, i.e., main trunk perpendicular, right main pulmonary artery parallel, and left main pulmonary artery oblique to the coronal imaging plane, causing possible different spin-tracer saturation effects in FAIR imaging in a coronal scan.

In other words, when the upstream artery exhibits a proportion β lying within the image slice, the resulting estimation of the tissue blood flow would be underestimated by a factor of β. One further notices that even if the derivations above were performed for a saturation recovery experiment, the same principle holds true, at least qualitatively, for all arterial spin labeling methods.

The FAIR technique has been used successfully used in transaxial brain imaging (9) because the blood supply is relatively unidirectional (caudocranially) below the skull base level, such that the inflowing blood can be regarded as completely tagged in the transaxial slice-selective inversion-recovery scan. In comparison, the vessels for inflowing blood for the lungs consist of the main pulmonary artery (or the pulmonary trunk) from the right cardiac ventricle, plus the subsequently branched right and left pulmonary arteries flowing into the right and left lungs, respectively (Fig. 1). These three major vessels are obviously oriented along very different directions. If FAIR were to be used in a coronal scan for lung perfusion, it is likely that for some slice locations, the image slice would contain a substantial portion of the upstream vessels, causing an effective "saturation of the spin-tracer" and thus a reduction in perfusion-related signal changes as shown in Eq. [9]. The above phenomenon is further anticipated to be prominent especially for the right lung, because the right pulmonary artery is along the left–right direction (Fig. 1) that is likely in-plane oriented in a coronal scan (i.e., a larger β). In contrast, performing sagittal scans may largely circumvent this tracer saturation effect.

Experiments—Part I: Intersequence Comparison between FAIR and CE-MRI

Subjects and Image Acquisition

A total of six healthy young adults (aged 23–28 years, all male) volunteered participation in this study. None of these participants had a history of pulmonary diseases. All subjects underwent FAIR imaging followed by CE-MRI performed on a 1.5-T MR system (General Electric Signa CVi, Milwaukee, WI). Coronal perfusion-weighted MR images were acquired following a transaxial localizer slightly

above the heart to see the relative locations of the right and left pulmonary arteries (Fig. 2). FAIR imaging was performed using an inversion-recovery-prepared single-shot fast spin-echo sequence (10,11), with TI = 1400 msec, effective TE = 27 msec, echo spacing = 4.58 msec, NEX = 15, matrix = 128 × 128 (half Fourier) and interpolated to 256 × 256 for display, and slice thickness = 10~12 mm with two coronal slices acquired sequentially (for slice locations see Fig. 2). Cardiac gating was used along with breath-holding on end-inspiration during each single excitation, such that motion-related influences were minimized in signal averaging. Note that cardiac gating was needed to ascertain consistent cardiac phase, not only to ensure the same shape and location of the heart in all images, but also because the amounts of blood flow from the right ventricle to the lungs during systole and diastole are substantially different. In FAIR imaging, cardiac gating was achieved by placing the excitation pulse at TD after the R-wave, where TD stands for trigger delay and was set in our study to 1.6 times the R–R interval. The inversion RF pulse was then placed at time TI before the excitation pulse, consistently for all signal averages. The inversion RF pulse was toggled between being slice-selective and slice-nonselective at a time separation of 5~6 sec to ensure complete T_1 recovery and interleaved within the 15 signal averages. Thickness of the inversion pulse was set at twice of the excitation pulse. Total imaging time for FAIR was about 3 min or less at each slice location.

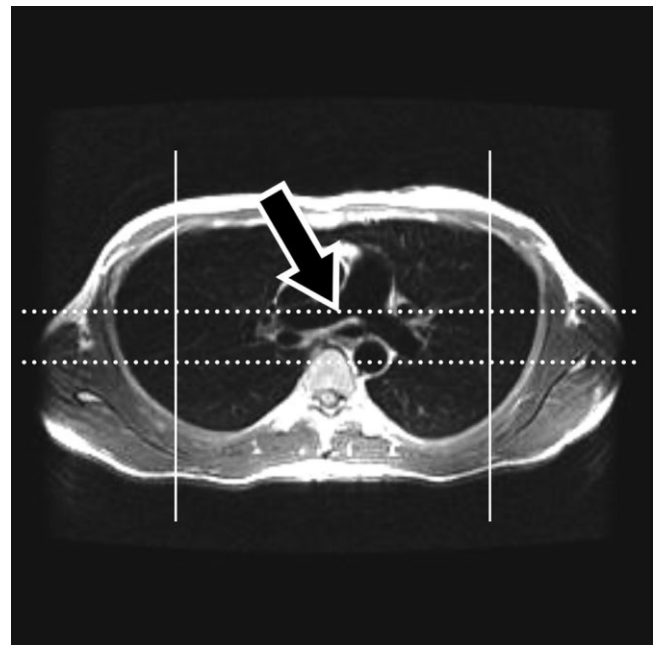Dynamic CE-MRI at the same slice locations as in FAIR was accomplished using an inversion-recovery-prepared

FIG. 2. Transaxial localizer from which the coronal image locations were determined. Dashed lines indicate the two coronal slice locations. Note that the middle slice covers a significant portion of the right pulmonary artery (open arrow), whereas the posterior slice does not include the upstream pulmonary arteries. The two vertical solid lines indicated the slice locations for the sagittal scans in the intrasequence comparison part of the study (see text for details).

segmented EPI technique (18) with TI/TR/TE/ETL = 180/6.5/1.2/4, matrix = 128 × 128 and interpolated to 256 × 256 for display, and slice thickness = 10~12 mm with two coronal slices acquired (identical to that used in FAIR for every subject). This sequence allows about four slices to be acquired in one cardiac cycle (18). A bolus of 0.05 mmol/Kg Gd-DTPA (Magnevist, Schering, Germany) was injected into the antecubital vein using an MR-compatible power injector at a speed of 3 mL/sec after the image acquisition started. Cardiac gating was also used together with breath-holding, again at end-inspiration, to avoid image misregistration. A total of 40~60 frames, separated by one R–R interval from one another, were obtained at each coronal slice location. Hence total imaging time for CE-MRI was less than a minute. For all healthy subjects included in our study, breath-holding during the first-pass transit of the contrast agent was successful. The subjects were in supine position throughout the entire examinations. The institutional review board in our hospital approved the imaging protocol.

Perfusion Calculation

Relative pulmonary blood flow (rPBF) maps were created on a voxel-by-voxel basis after image acquisition. For the FAIR method, rPBF maps were calculated by a subtraction of the tagged and control images (10,11). For the generation of rPBF maps using the dynamic CE-MRI images, the signal intensity-time curves for all voxels within the lungs were first extracted and baseline intensity subtracted. γ-Fitting was performed to remove the recirculation effects, following which the rPBF was obtained using the central volume principle given by rPBF = rPBV/rMTT, where rPBV, the relative pulmonary blood volume, was estimated by an integration of the γ-fitted signal intensity-time curve (assuming changes in signal intensity approximately proportional to contrast concentration) and rMTT, the mean transit time, was computed as the normalized first moment of the signal intensity-time curve (13,16).

Data Analysis

Comparison of the two types of rPBF maps was accomplished using region-of-interest (ROI) analysis. For this purpose, 20 ROIs (10 each in the left and right lungs), each about 200 voxels in size, were selected in the pulmonary parenchyma on each coronal image slice. Large vessels showing obviously too high rPBF values were avoided by comparing individual voxel values with an rPBF threshold. Voxels with rPBF values larger than the threshold were excluded from the ROI analysis. Regions near the fissure were also avoided as rPBF is expected to be intrinsically smaller than in the pulmonary parenchyma. Care was taken such that the selection of ROIs was roughly symmetric in the two lungs in order to allow right-to-left comparisons, because neither of our two perfusion techniques provided PBF information in an absolutely quantitative manner. Following selections of the ROIs, the right-to-left rPBF ratio was defined as R = (rPBF of ROI in the right lung)/(rPBF of ROI in the left lung). The ratios obtained from the FAIR and the CE-MRI rPBF maps were denoted R_{FAIR} and $R_{\text{CE-MRI}}$, respectively, with ROIs de-fined on CE-MRI rPBF maps copied to FAIR rPBF maps to ensure identical ROI locations. Therefore, 20 rPBF ratios (10 R_{FAIR}'s and 10 $R_{\text{CE-MRI}}$'s) were obtained per slice on every subject. Subsequently, 10 values of $R_{\text{FAIR}}/R_{\text{CE-MRI}}$ were derived for each slice. Note that in the ideal situation where both FAIR and CE-MRI provide accurate perfusion information, R_{FAIR} and $R_{\text{CE-MRI}}$ are expected to be equal.

Statistical Analysis

The overall difference between R_{FAIR} and $R_{\text{CE-MRI}}$ for the six subjects (total 60 ROI pairs in each of the two slice locations) was investigated separately for the middle and posterior slices using paired Student's t test. A P value of 0.05 or smaller was regarded as statistically significant. Note that the paired t test was used because the ROI pairs on different coronal slice locations are nearly identical in terms of their locations along both the superior–inferior and the left–right directions. The overall agreement between R_{FAIR} and $R_{\text{CE-MRI}}$ for the six subjects was assessed using the intraclass correlation coefficient (19), which produces measures of consistency or agreement of values within cases, i.e., rPBF measurements obtained using FAIR and CE-MRI within a same case in this study. This overall agreement was again examined separately for the two slice locations. In addition, a graphical visualization of the agreement between R_{FAIR} and $R_{\text{CE-MRI}}$ was assessed using the Bland–Altman analysis (20).

Experiments—Part II: Intrasequence Comparison with FAIR

Effects of Slice Orientations

To provide further evidence of the location-dependent tracer saturation effects in FAIR imaging, an additional three subjects (aged 21–26 years, all male) were recruited for the second part of the study. Coronal and sagittal FAIR images were obtained in separate scans. Two slices were acquired for the coronal scan, with slice locations indicated as in Fig. 2 (middle and posterior, in order to illustrate different tracer saturation effects). For the sagittal scan, two more slices were obtained: one acquired crossing the right lung and the other crossing the left lung (solid lines in Fig. 2), respectively, to allow for left and right comparison. Care was taken such that the transmitter and receiver gains were kept identical for all scans. The values of rPBF, calculated using the method as detailed previously, were then compared for each pair of orthogonal images on the intersected column of voxels. Ideally, perfusion estimation should be independent of the slice orientations if β (Eq. [9]) is the same. We hypothesized that (1) sagittal planes have similar β at the right slice versus the left slice; (2) the posterior coronal plane have similar β for both lungs to that in the sagittal planes; and (3) the middle coronal plane have β values that are higher for the right lung than for the left lung, since the middle coronal planes included the upstream right pulmonary artery within the imaging slice. Therefore, a comparison of pulmonary blood flow at the same voxels measured by coronal FAIR versus sagittal FAIR, respectively, would provide an "intrasequence" comparison to test the phenomenon of slice-location-dependent tracer saturation effect.

Table 1
R_{FAIR}/R_{CE-MRI} Values (Mean $\pm$ std from 10 ROI Pairs) Listed for the Six Subjects in Different Slice Locations

R_{FAIR}/R_{CE-MRI}	Subject 1	Subject 2	Subject 3	Subject 4	Subject 5	Subject 6
Posterior slice	1.00 $\pm$ 0.14	0.96 $\pm$ 0.15	0.92 $\pm$ 0.10	1.03 $\pm$ 0.20	0.89 $\pm$ 0.10	1.06 $\pm$ 0.21
Middle slice	0.69 $\pm$ 0.19	0.55 $\pm$ 0.15	0.70 $\pm$ 0.10	0.64 $\pm$ 0.22	0.70 $\pm$ 0.18	0.89 $\pm$ 0.15
Underestimation for middle slice (%)	31	43	34	38	21	16

Note. In the ideal situation where both FAIR and CE-MRI provide accurate perfusion information, R_{FAIR} and R_{CE-MRI} are expected to be equal and their ratio should be close to unity for healthy subjects. Note that compared with R_{FAIR}/R_{CE-MRI}'s for the posterior slice, in the middle slice R_{FAIR}/R_{CE-MRI}'s were substantially smaller on all subjects.

The data analysis for this part of study consisted of the following steps. The coronal rPBF values were plotted in a voxel-by-voxel manner against the sagittal rPBF values in a scatter plot, for the caudocranial voxel columns intersected by two orthogonal slices (total four pairs). The locations of the intersecting columns were identified in the coronal and sagittal images using anatomic coordinate values indicated on the transaxial localizer (Fig. 2). Note that the imaging voxels were highly anisotropic in the FAIR images, with slice thickness three times larger than the in-plane voxel width before zero-filled interpolation. As a consequence, the voxel columns intersected by two orthogonal slices were constructed by averaging rPBF values from three adjacent voxels. The overall agreements between coronal and sagittal rPBF values were assessed using the intraclass correlation coefficient R_I for the four pairs of intersecting imaging slices, respectively.

Effects of the Inversion Time TI

We hypothesized that the tracer saturation effect arises mainly from an inclusion of upstream vessel by the imaging slice. Hence, its existence is anticipated to be largely independent of the inversion time TI, except that the right-to-left discrepancy may somehow reduce at very long TI due to T_1-relaxation-induced loss of the labeled tracers (11). The possible influences of TI on the tracer saturation effects were experimentally investigated on two healthy subjects using coronal FAIR imaging at three different TI values (1000, 1400, and 1800 msec), with results compared with data obtained from CE-MRI. For this purpose, R_{FAIR} and R_{CE-MRI} were derived from 20 ROIs in each slice (10 ROIs in each lung, as described in a previous section, Experiment Part I) and their ratios calculated (10 R_{FAIR}/R_{CE-MRI} values in each slice from the 10 ROI pairs). Results were plotted separately for the posterior and middle slices. Ideally in the absence of tracer saturation effects, the FAIR to CE-MRI perfusion ratio (R_{FAIR}/R_{CE-MRI}) should be close to unity. Differences in R_{FAIR}/R_{CE-MRI} between the posterior and middle slices were assessed using Student's t test, with P value of 0.05 or smaller regarded as statistically significant.

RESULTS

Intersequence Comparison between FAIR and CE-MRI

Table 1 listed the ratios R_{FAIR}/R_{CE-MRI} (mean $\pm$ std for 10 ROI pairs) in different slice locations for each subject. As seen in Table 1, in the posterior image slice, the values of R_{FAIR}/R_{CE-MRI} were close to unity in all of our cases. Thus,

FAIR and CE-MRI provided basically consistent rPBF information at the posterior slice location. In the middle slice location, however, the R_{FAIR}/R_{CE-MRI} values were substantially lowered, suggesting 16~43% underestimation of FAIR-derived rPBF in the right lung than the CE-MRI method. The inconsistency of FAIR and CE-MRI perfusion in the middle slice is clearly at variance to the situation in the posterior slice.

The phenomena mentioned above could also be depicted in the rPBF maps. Figure 3a and b shows the coronal rPBF maps of a 23-year-old male subject acquired using FAIR and CE-MRI, respectively, from a posterior slice location (for slice locations see Fig. 2). These two images visually showed no evident difference in pulmonary perfusion between the right and the left lungs. Figure 4a and b shows the coronal FAIR and CE-MRI rPBF maps of the same subject acquired from a middle slice location. In contrast to the similar image appearance for Fig. 3a and b, the FAIR rPBF map in Fig. 4a demonstrated substantially lower perfusion in the right lung (open arrow) than the contralateral side in the left lung (long arrow). On the other hand, the CE-MRI rPBF map in Fig. 4b of the same subject indicated that there was no evident visual difference in the perfusion for the right and left lungs.

The association between R_{FAIR} and R_{CE-MRI} for the two slice locations is shown in Fig. 5 for the 60 ROI pairs from the six subjects recruited in our study. R_{FAIR}'s were in general smaller than R_{CE-MRI}'s in the middle slice, but not in the posterior slice. The mean difference between R_{FAIR} and R_{CE-MRI} for the posterior coronal slice was -0.02 and did not reach statistical significance (paired Student's t test, $P = 0.115$). The intraclass correlation coefficient (19) assessing the absolute agreement between R_{FAIR} and R_{CE-MRI} was $R_I = 0.78$. The 95% confidence interval was [0.67, 0.86]. A Bland–Altman plot (20) showed that the disagreement between R_{FAIR} and R_{CE-MRI} was less than 0.27 within two standard deviations (Fig. 6a; mean difference of -0.02, upper and lower limits at 0.22 and -0.27, respectively). For the middle coronal slice, however, the mean difference between R_{FAIR} and R_{CE-MRI} for the 60 ROI pairs was -0.38, which was statistically significant (paired Student's t test, $P = 0.000$). Intraclass correlation coefficient R_I was only 0.34, with 95% confidence interval equal to [-0.09, 0.68], suggesting that FAIR showed a substantially lower perfusion in the right lung compared with CE-MRI. Bland–Altman analysis showed a preferential lower R_{FAIR} than R_{CE-MRI} by -0.38 and a prominent disagree-
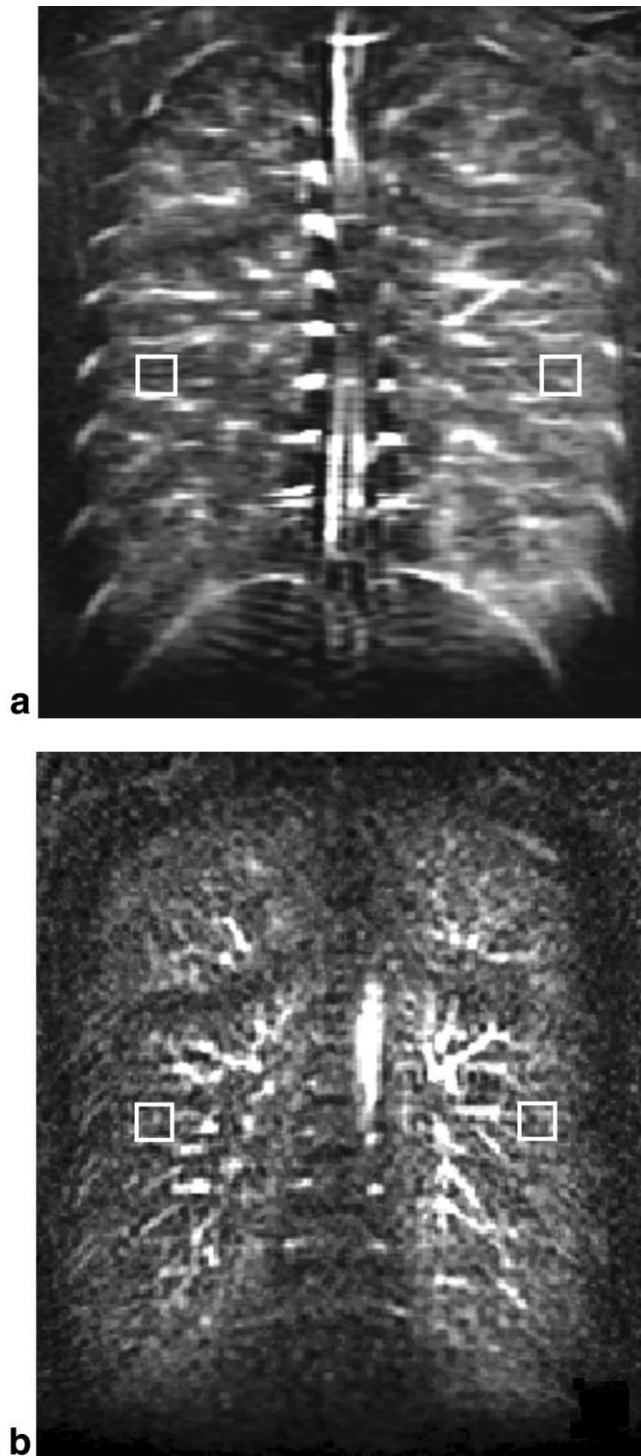
FIG. 3. Coronal rPBF maps of the posterior slice from a 23-year-old male subject obtained using (**a**) the FAIR (rPBF derived from a subtraction of the tagged and control images) and (**b**) the CE-MRI techniques (rPBF derived using central volume principle from the γ-fitted first-pass Gd-bolus transit), respectively. With regions of large vessels excluded, the exemplified rectangular regions-of-interest (white boxes) yielded $R_{FAIR} = 0.84$ and $R_{CE-MRI} = 0.85$, suggesting that FAIR and CE-MRI provide consistent information in pulmonary perfusion.

ment (Fig. 6b; mean difference of -0.38, upper and lower limits at 0.04 and -0.80, respectively).

Intrasequence Comparison with FAIR

Figure 7 demonstrated the comparison of rPBF obtained using FAIR with different slice orientations. In Fig. 7a it is seen that for the posterior coronal slice, rPBF values were consistent with those obtained using sagittal scans for both
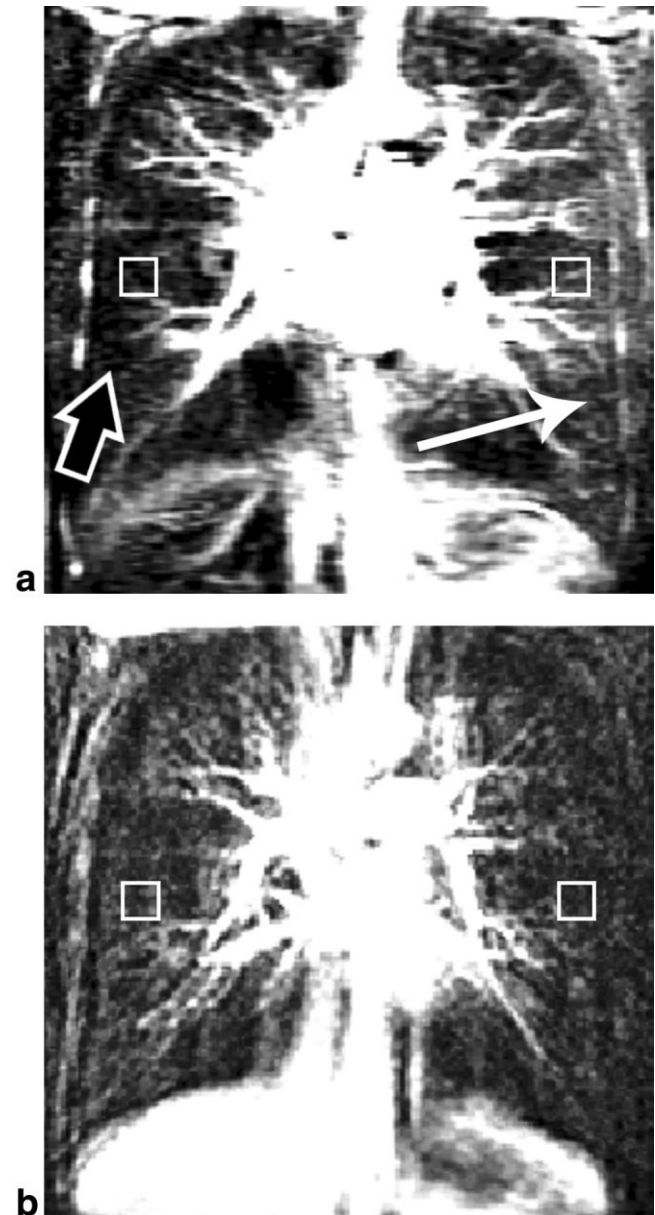

FIG. 4. Coronal rPBP maps of the middle slice from a 23-year-old male subject (the same as in Fig. 3) obtained using (**a**) the FAIR and (**b**) the CE-MRI techniques, respectively. In a, the pulmonary blood flow in the right lung (e.g., open arrow) appears substantially lower than in the left lung (e.g., long arrow). In contrast, the CE-MRI rPBF map in b shows no obvious right-to-left perfusion difference. The exemplified rectangular regions-of-interest (white boxes) yielded $R_{FAIR} = 0.62$ and $R_{CE-MRI} = 0.99$, respectively. The disagreement between rPBF maps obtained from the two methods in the middle image slice is clearly seen.

FIG. 5. Right-to-left rPBF ratios R_{FAIR} plotted versus R_{CE-MRI} from 60 ROI pairs in each slice for six healthy subjects. In the posterior slice, R_{FAIR} agrees well with R_{CE-MRI} by showing consistent values with a regression line of $y = 0.97x$ (filled circles). The intraclass correlation coefficient was $R_I = 0.78$. On the contrary, R_{FAIR} tends to be lower than R_{CE-MRI} ($y = 0.69x$; open circles) in the middle slice, with intraclass correlation coefficient $R_I = 0.34$.
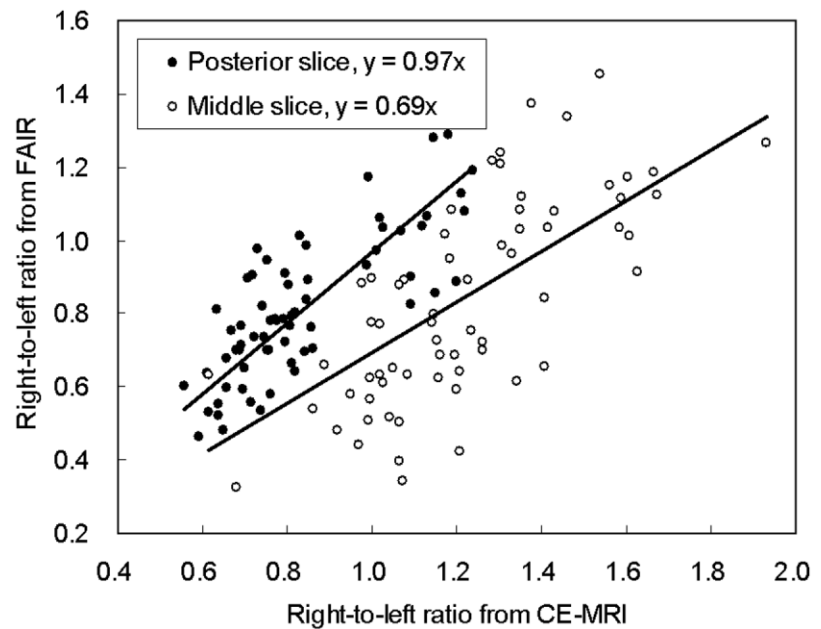
the right and the left lungs (regression slopes both close to unity; intraclass correlation coefficients = 0.90 and 0.91 for the right and left lungs, with 95% confidence intervals being [0.86, 0.94] and [0.87, 0.94], respectively). For the middle coronal slice, however, Fig. 7b showed that the rPBF values estimated from the coronal FAIR image were in good agreement with their sagittal counterpart only for the left lung (regression slope = 1.11; intraclass correlation coefficient $R_I = 0.89$; 95% confidence interval = [0.83, 0.92]). For the right lung, coronal rPBF values were in general lower than sagittal rPBF by about 22% on the average (regression slope = 0.78; intraclass correlation coefficient $R_I = 0.79$; 95% confidence interval = [0.70, 0.85]).

Figure 8 shows the FAIR images acquired with different TI values (top row, posterior slices; bottom row, middle slices; from left to right: TI = 1000, TI = 1400, and TI = 1800 msec, respectively). As visually demonstrated, the posterior coronal slices did not exhibit seemingly reduced perfusion in the right lung (Fig. 8a–c). The tracer saturation effects in the middle slices, on the other hand, can be seen regardless of the TI values chosen (Fig. 8 d–f). Perfusion ratios (R_{FAIR}/R_{CE-MRI}) for the six images are plotted in Fig. 9, with values derived from interrogated ROI pairs as selected using the approach described in the aforementioned Method for Experiment Part I. The differences between R_{FAIR}/R_{CE-MRI} obtained from the posterior slices and those from middle slices were all statistically significant, with the *P* values increasing with increase in TI.

DISCUSSION AND CONCLUSIONS

Recent technical developments have rendered MR imaging to play an increasingly important role in the monitoring of the respiratory system (3–5,7,12,13,21,22). Although proton MR imaging compared poorly in signal-to-noise ratio to imaging using hyperpolarized idle gas (21,22), proton MR imaging in the lungs does not necessitate substantial

hardware and software system modifications and is hence directly applicable in clinical practice (3–5,7,12,13). Even if proton MR imaging may not entirely substitute for nuclear medicine scintigraphy, which is the current standard for perfusion imaging in the lungs, the ability to obtain information on rPBF at high spatial resolution in a short time has demonstrated strong clinical potential of perfusion MR in the pulmonary system.

The FAIR technique for pulmonary perfusion imaging, as well as other variants of the arterial spin labeling methods, is uniquely advantageous in its use of the endogenous tracer, which is particularly suitable in situations where repeated examinations are needed (15). One recent study comparing a FAIR-based spin labeling method with CE-MRI concluded that the perfusion parameters obtained with the two modalities were generally in good agreement (14). Results from our study indicate, however, that the FAIR-derived perfusion maps could substantially underestimate the rPBF in the right lung by 16 to 43% (Table 1), with obvious difference that is visually perceivable (Fig. 4a). In addition, this estimation error depends on slice locations, i.e., being more severe at the middle than posterior coronal images. This result of underestimated rPBF in the right lung for the middle slice is consistent with our inference of the spin-tracer saturation effects as detailed in a previous section. Going back to Fig. 2, the two coronal image slices acquired for rPBF calculation in this study are located covering the right pulmonary artery (the middle slice) and posterior to the two pulmonary arteries (the posterior slice), respectively. For the flow-sensitive (i.e., tagged) images in FAIR, the in-plane right pulmonary artery experiences a substantial amount of spin inversion when imaging the middle coronal slice, in contrast to the expected situation where the upstream "labeled" spins should be noninverted and close to the thermal equilibrium magnetization. Consequently, the FAIR-derived rPBF in the right lung is significantly underestimated. On the other hand, the tracer saturation effect for the left pulmo-
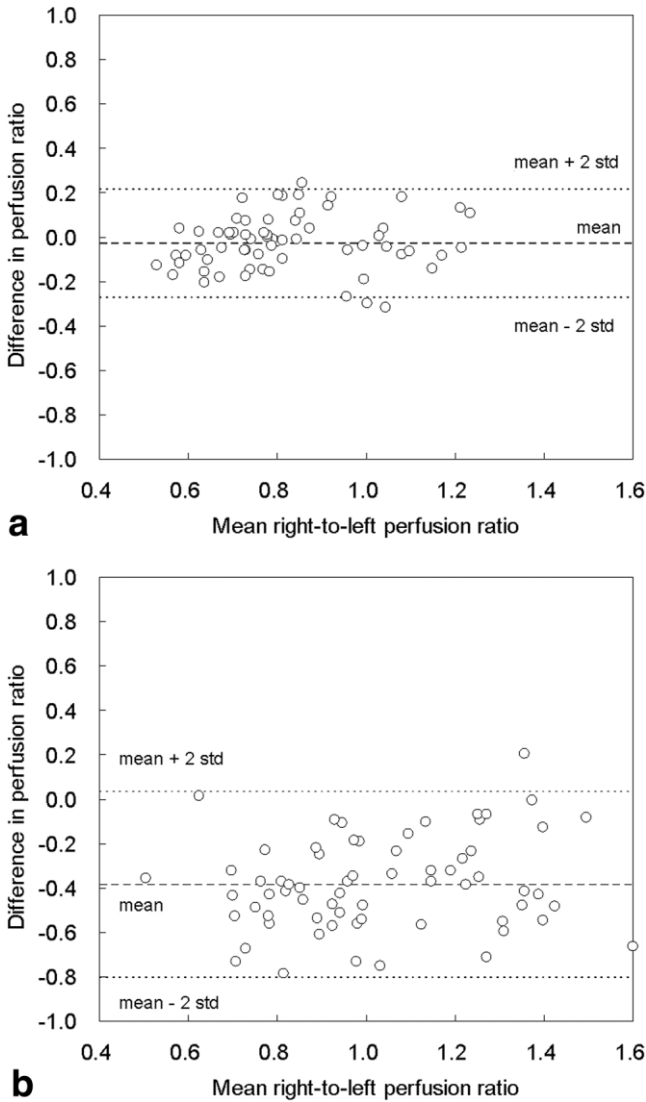
FIG. 6. Bland–Altman analysis plots to assess the agreement between rPBF ratios obtained from all six subjects using FAIR and CE-MRI for the posterior (**a**) and middle (**b**) coronal slices, respectively. In a, the center dashed line indicates the mean percentage disagreement (defined as $R_{FAIR} - R_{CE-MRI}$ divided by the mean of R_{FAIR} and R_{CE-MRI}) at -0.02, whereas the upper and lower dotted lines show that the disagreements within two standard deviations are within 0.22 and -0.27, respectively. Hence, for the posterior slice, rPBF ratios derived from FAIR and CE-MRI show fairly good agreements. For the middle slice, however, the mean percentage disagreement shown in b is at -0.38, suggesting substantial underestimation of rPBF in the right lung by the FAIR method.

nary artery is expected to be less prominent, due to relatively oblique vessel orientation. Hence, perfusion underestimation for the left lung, if present, should be much less in extent than for the right lung. In contrast to the middle slice, the posterior coronal slice does not contain the upstream vessels. The spin-tracer saturation effect is absent. Thus, no underestimation of perfusion is seen in the rPBF maps obtained from FAIR imaging, similar to what was reported in a recent study showing comparison on posterior coronal image slices (14). In such circumstances, FAIR

and CE-MRI provide consistent information in pulmonary perfusion by showing intraclass correlation coefficient R_I of 0.78 (95% confidence interval [0.67, 0.86]).

In order to verify that the discrepancy between FAIR and CE-MRI did not root from artifactual origins other than the inflow tracer saturation effect, we acquired sagittal FAIR images to compare with coronal FAIR images to examine the intrasequence relationship of scan location versus perfusion measurements. If such a discrepancy originated from, for instance, imperfect distribution of the RF flip angle within a large field-of-view,
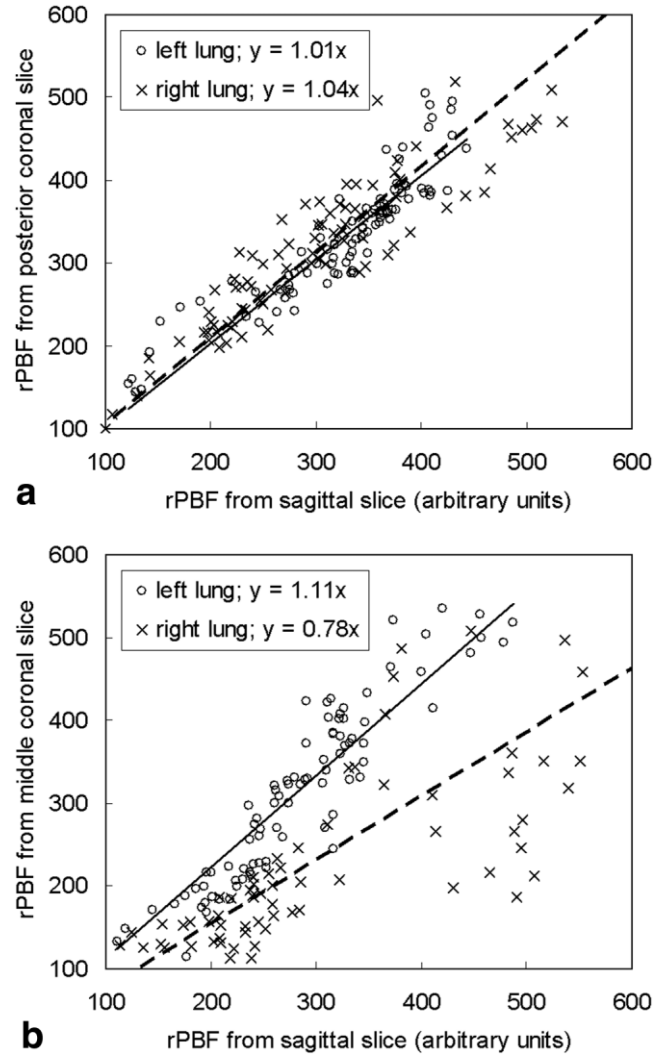

FIG. 7. Scatter plots showing the rPBF estimated from posterior (**a**) and middle (**b**) coronal FAIR images, plotted against values measured from sagittal FAIR images at the same voxel locations with identical transmitter and receiver gains in the left lung (circles; solid regression lines) and right lung (crosses; dashed regression lines), respectively. The rPBF values obtained from the posterior coronal slice were in good agreement with those from the sagittal slice for both lungs, showing regression slopes close to unity with intraclass correlation coefficients both greater than $R_I = 0.90$ (a). The middle coronal rPBF, however, showed consistency with sagittal rPBF in the left lung only ($R_I = 0.89$), with coronal values lower than sagittal by 22% on the average (regression slope 0.78; $R_I = 0.79$) in the right lung (b).

FIG. 8. Coronal FAIR images acquired with different TI values (top row, posterior slices; bottom row, middle slices; from left to right: TI = 1000, TI = 1400, and TI = 1800 msec, respectively). The posterior slices did not visually exhibit reduced perfusion in the right lung (**a–c**). On the other hand, the tracer saturation effects in the right lung (arrows) can be seen in the middle slices regardless of the TI values chosen (**d–f**).
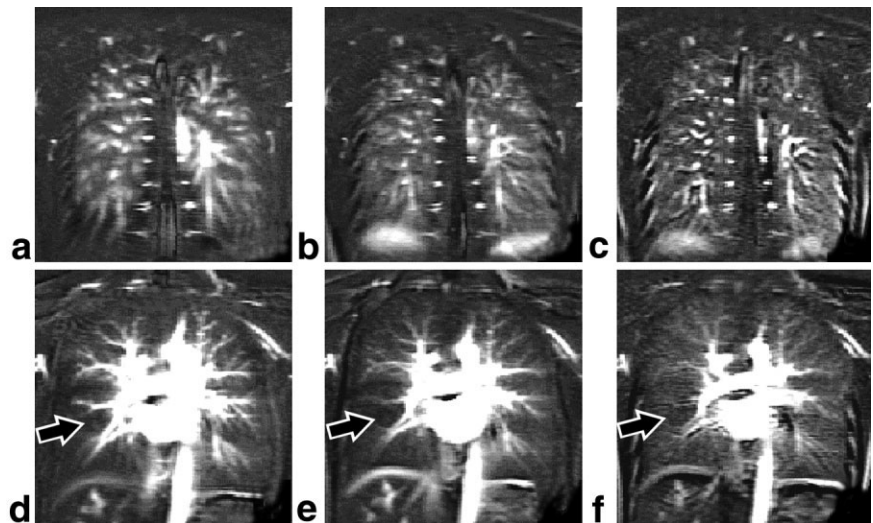
the sagittal FAIR images would show similar regional disagreement in perfusion estimations. In our experiments, we observed lower rPBF only for the right lung on middle coronal FAIR images, not in any of the sagittal planes or in the posterior coronal slice. The intrasequence comparison results hence provided a reinforcing evidence of the tracer saturation effects and essentially ruled out other artifactual causes.

The presence of inflow tracer saturation effect in FAIR has several implications in pulmonary perfusion MR imaging. The first issue is the expected limited slice coverage confined to posterior coronal slices where the spin-tracer saturation effects are largely absent. Limitation in slice coverage could be detrimental, especially for clinical di-

agnosis because whole-lung imaging is often desirable. Performing, e.g., sagittal scans may circumvent rPBF underestimation in the right lung for arterial spin-labeling techniques (4), which, however, may not be a preferential solution in clinical practice because the number of slices would need to be substantially increased to cover the entire lungs. Even if three-dimensional sagittal scanning in one lung has been shown to be effective in revealing focal perfusion deficits (4), right-to-left comparison would not be directly accessible in sagittal imaging. Note that right-to-left comparison of pulmonary perfusion is especially important clinically for preoperative evaluation of lung function, such as candidate selection for lung transplantation, volume reduction surgery (23), and postoperative evaluation of lung functions on patients with congenital heart diseases (24). Therefore, coronal imaging capability is a highly desirable feature in clinical practice.

Since the tracer saturation effects as indicated in Eqs. [6] to [9] apply in general to all perfusion imaging methods based on arterial spin labeling, a reasonable extrapolation of the results from our study would suggest that other techniques such as QUIPSS II (25) are likely to be susceptible to the same pitfalls when applied to coronal perfusion imaging of the lungs. Furthermore, the presence of tracer saturation effects is relatively independent of the inversion time (or the inflow time) TI (Figs. 8 and 9), as long as the TI values are appropriately chosen (on the order of 1400 msec) to reflect perfusion within the pulmonary parenchyma. However, there appears a trend that the saturation effect diminished while the TI was elongated, as seen in Fig. 9. This result is consistent with the inherent effects of tracer loss due to T_1 relaxation and therefore reduces the contrast-to-noise ratio for FAIR imaging (11). In other words, the measurement discrepancy in pulmonary perfusion seen on middle coronal FAIR images may become obscured at longer TI (>1800 ms), which is, however, not a recommended option because of the expected reduction in perfusion sensitivity.

In contrast to FAIR, the rPBF maps obtained with CE-MRI from the healthy subjects included in our study did not show similar right-to-left difference. The R_{CE-MRI} val-
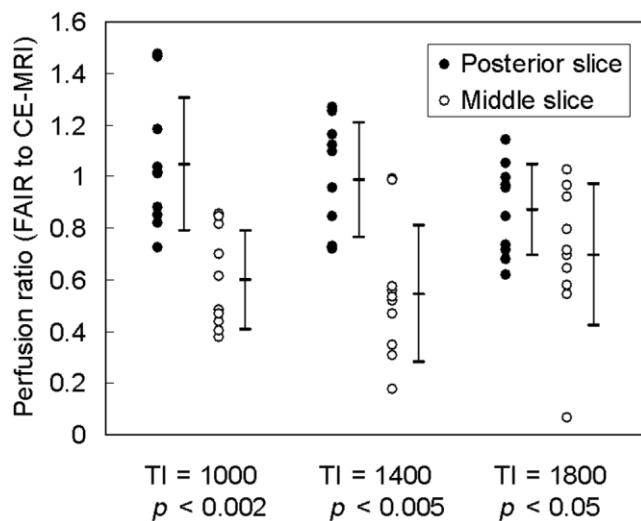

FIG. 9. Right-to-left perfusion ratios derived from FAIR images acquired using three different TI values, expressed as the ratios to values obtained from CE-MRI, for interrogated ROI pairs as selected from Fig. 8 using the approach described under Methods. The circles were the individual values, with error bars (mean ± std) on their right-hand-side. Differences between perfusion ratios obtained from the posterior slices and those from middle slices were all statistically significant.

ues were mostly not too far from unity, as is expected for healthy subjects, regardless of the coronal slice locations. Note that one may argue that in perfusion scintigraphy of normal subjects, the total perfusion volume of the right lung may be larger than that of left lung. However, this difference is simply due to the fact that the left lung is usually smaller in the presence of the left-sided heart. By using the regional perfusion analysis in our study, i.e., ROI to ROI comparison, the influence of total lung volume could be eliminated and therefore the right-to-left ratio should be close to unity in normal subjects. In addition to the values of R_{CE-MRI} in accordance with expectation, imaging of pulmonary perfusion using CE-MRI is advantageous in that it is considered relatively mature, with PBF calculation validated using invasive methods in animal models (13,17) and its clinical value widely demonstrated (6–8,12,26–28). At least in our limited scale of study, no technical pitfalls in CE-MRI perfusion were found. The experimental results in Fig. 7 obtained using only FAIR imaging further indicated that the perfusion underestimation was inherent in coronal FAIR imaging but not related to CE-MRI.

One relatively minor issue further favoring the use of CE-MRI to assess pulmonary perfusion is the point-spread-function blurring shown in the FAIR rPBF images (Figs. 3a and 4a). In this study, the half-Fourier single-shot fast spin-echo scheme was used as the signal readout module after the inversion-recovery preparation, with center-out phase encoding order. Since the lung parenchyma and the pulmonary vessels have relatively short T_2 compared with the total length of the data acquisition window (on the order of a second or less), a relaxation-induced attenuation of the high-spatial-frequency components at the outer part of the k-space could lead to significant point-spread-function blurring (29). The blurring was visually prominent for the FAIR rPBF maps in both Figs. 3a and 4a along the left–right direction (i.e., the phase encoding direction), compared with the CE-MRI rPBF maps in Figs. 3b and 4b. Fortunately, the point-spread-function blurring was not a severe problem in terms of ROI analysis of rPBF in our study. It is further noted that the blurring issue is related only to the signal readout module, rather than the intrinsic difference in the contrast preparation schemes between FAIR and CE-MRI.

We conclude that FAIR and CE-MRI provide consistent rPBF estimations only in the absence of the inflow tracer saturation effects. If coronal slices were taken, as preferentially performed for clinical lung imaging, FAIR would result in substantial rPBF underestimation in the right lung when the image slice covers the upstream right pulmonary artery. For whole-lung coverage, therefore, CE-MRI compares favorably to FAIR in the assessment of pulmonary perfusion. The FAIR technique should be carefully exercised in clinical practice to avoid misleading interpretations and diagnosis.

REFERENCES

1. Lewis DH, Kott B, Jacobson AF. Single-photon emission tomography imaging of the chest. Respir Care 2001;46:940–945.
2. Hatabu H, Gaa J, Kim D, Li W, Prasad PV, Edelman RR. Pulmonary perfusion: dynamic contrast-enhanced MRI using ultra-short TE and inversion recovery turbo FLASH. Magn Reson Med 1996;36:503–508.
3. Amundsen T, Kvaerness J, Jones RA, Waage A, Bjermer L, Nilsen G, Haraldseth O. Pulmonary embolism: detection with MR perfusion imaging of lung–a feasibility study. Radiology 1997;203:181–185.
4. Roberts DA, Gefter WB, Hirsch JA, Rizi RR, Dougherty L, Lenkinski RE, Leigh JS Jr, Schnall MD. Pulmonary perfusion: respiratory-triggered three-dimensional MR imaging with arterial spin tagging–preliminary results in healthy volunteers. Radiology 1999;212:890–895.
5. Uematsu H, Levin DL, Hatabu H. Quantification of pulmonary perfusion with MR imaging: recent advances. Eur J Radiol 2001;37:155–163.
6. Amundsen T, Torheim G, Kvistad KA, Waage A, Bjermer L, Nordlid KK, Johnsen H, Asberg A, Haraldseth O. Perfusion abnormalities in pulmonary embolism studied with perfusion MRI and ventilation-perfusion scintigraphy: an intra-modality and inter-modality agreement study. J Magn Reson Imaging 2002;15:386–394.
7. Lehnhardt S, Thorsten Winterer J, Strecker R, Hogerle S, Herget G, Geens V, Laubenberger J, Uhrmeister P. Assessment of pulmonary perfusion with ultrafast projection magnetic resonance angiography in comparison with lung perfusion scintigraphy in patients with malignant stenosis. Invest Radiol 2002;37:594–599.
8. Berthezene Y, Croisille P, Wiart M, Howarth N, Houzard C, Faure O, Douek P, Amiel M, Revel D. Prospective comparison of MR lung perfusion and lung scintigraphy. J Magn Reson Imaging 1999;9:61–68.
9. Kim SG. Quantification of relative cerebral blood flow change by flow-sensitive alternating inversion recovery (FAIR) technique: application to functional mapping. Magn Reson Med 1995;34:293–301.
10. Mai VM, Berr SS. MR perfusion imaging of pulmonary parenchyma using pulsed arterial spin labeling techniques: FAIRER and FAIR. J Magn Reson Imaging 1999;9:483–487.
11. Mai VM, Liu B, Polzin JA, Li W, Kurucay S, Bankier AA, Knight-Scott J, Madhav P, Edelman RR, Chen Q. Ventilation-perfusion ratio of signal intensity in human lung using oxygen-enhanced and arterial spin labeling techniques. Magn Reson Med 2002;48:341–350.
12. Amundsen T, Torheim G, Waage A, Bjermer L, Steen PA, Haraldseth O. Perfusion magnetic resonance imaging of the lung: characterization of pneumonia and chronic obstructive pulmonary disease. A feasibility study. J Magn Reson Imaging 2000;12:224–231.
13. Hatabu H, Tadamura E, Levin DL, Chen Q, Li W, Kim D, Prasad PV, Edelman RR. Quantitative assessment of pulmonary perfusion with dynamic contrast-enhanced MRI. Magn Reson Med 1999;42:1033–1038.
14. Wang T, Schultz G, Hebestreit H, Hebestreit A, Hahn D, Jakob PM. Quantitative perfusion mapping of the human lung using 1H spin labeling. J Magn Reson Imaging 2003;18:260–265.
15. Roberts DA, Rizi RR, Lipson DA, Ferrante MA, Bearn L, Rolf L, Baumgardner J, Yamomoto A, Hatabu H, Hansen-Flaschen J, Gefter WB, Schnall MD. Dynamic observation of pulmonary perfusion using continuous arterial spin-labeling in a pig model. J Magn Reson Imaging 2001;14:175–180.
16. Levin DL, Chen Q, Zhang M, Edelman RR, Hatabu H. Evaluation of regional pulmonary perfusion using ultrafast magnetic resonance imaging. Magn Reson Med 2001;46:166–171.
17. Chen Q, Levin DL, Kim D, David V, McNicholas M, Chen V, Jakob PM, Griswold MA, Goldfarb JW, Hatabu H, Edelman RR. Pulmonary disorders: ventilation- perfusion MR imaging with animal models. Radiology 1999;213:871–879.
18. Slavin GS, Wolff SD, Gupta SN, Foo TKF. First-pass myocardial perfusion MR imaging with interleaved notched saturation: feasibility study. Radiology 2001;219:258–263.
19. Williamson JM, Lipsitz SR, Manatunga AK. Modeling kappa for measuring dependent categorical agreement data. Biostatistics 2000;1:191–202.
20. Bland JM, Altman DG. Statistical methods for assessing agreement between two methods of clinical measurement. Lancet 1986;1:307–310.
21. Moller HE, Chen XJ, Saam B, Hagspiel KD, Johnson GA, Altes TA, de Lange EE, Kauczor HU. MRI of the lungs using hyperpolarized noble gases. Magn Reson Med 2002;47:1029–1051.
22. Kauczor HU. Current issues in hyperpolarized gases in MRI: biomedical investigations and clinical applications. NMR Biomed 2000;13:173–175.
23. Johkoh T, Muller NL, Kavanagh PV, Cartier Y, Mayo JR, Tomiyama N, Murakami T, Naito H, Nakamura H, Moriya H. Scintigraphic and MR perfusion imaging in preoperative evaluation for lung volume reduction surgery: pilot study results. Radiat Med 2000;18:277–281.

24. Fratz S, Hess J, Schwaiger M, Martinoff S, Stern H. More accurate quantification of pulmonary blood flow magnetic resonance imaging than by lung perfusion scintigraphy in patients with Fontan circulation. Circulation 2002;106:1510–1513.

25. Wong EC, Buxton RB, Frank LR. Quantitative imaging of perfusion using a single subtraction (QUIPSS and QUIPSS II). Magn Reson Med 1998;39:702–708.

26. Iwasawa T, Saito K, Ogawa N, Ishiwa N, Kurihara H. Prediction of postoperative pulmonary function using perfusion magnetic resonance imaging of the lung. J Magn Reson Imaging 2002;15:685–692.

27. Matsuoka S, Uchiyama K, Shima H, Terakoshi H, Nojiri Y, Oishi S, Ogata H. Detectability of pulmonary perfusion defect and influence of breath holding on contrast-enhanced thick-slice 2D and on 3D MR pulmonary perfusion images. J Magn Reson Imaging 2001;14:580–585.

28. Carr JC, Laub G, Zheng J, Pereles FS, Finn JP. Time-resolved three-dimensional pulmonary MR angiography and perfusion imaging with ultrashort repetition time. Acad Radiol 2002;9:1407–1418.

29. Mulkern RV, Wong ST, Winalski C, Jolesz FA. Contrast manipulation and artifact assessment of 2D and 3D RARE sequences. Magn Reson Imaging 1990;8:557–566.